### **OPEN ACCESS**



# The Orbit and Mass of the Cepheid AW Per\*

Nancy Remage Evans 1, Alexandre Gallenne 2,3, Pierre Kervella 4, Antoine Mérand 5, John Monnier 6, John Monnie Richard I Anderson<sup>7</sup>, H. Moritz Günther<sup>8</sup>, Charles Proffitt<sup>9</sup>, Elaine M. Winston<sup>10</sup>, Grzegorz Pietrzynski<sup>11</sup>, Wolfgang Gieren 11, Joanna Kuraszkiewicz 12, Narsireddy Anugu 13, Rachael M. Roettenbacher 6, Cyprien Lanthermann 13, Mayra Gutierrez<sup>6,13</sup>, Gail Schaefer<sup>13</sup>, Benjamin R. Setterholm<sup>14</sup>, Noura Ibrahim<sup>6</sup>, and Stefan Kraus<sup>15</sup> <sup>2</sup> Instituto de Astrofísica, Departamento de Ciencias Físicas, Facultad de Ciencias Exactas, Universidad Andrés Bello, Fernández Concha 700, Las Condes, Santiago, Chile <sup>3</sup> French-Chilean Laboratory for Astronomy, IRL 3386, CNRS, Casilla 36-D, Santiago, Chile <sup>4</sup> LESIA, Observatoire de Paris, Université PSL, CNRS, Sorbonne Université, Université de Paris, 5 Place Jules Janssen, 92195 Meudon, France European Southern Observatory, Karl-Schwarzschild-Str. 2, 85748 Garching, Germany <sup>6</sup> Department of Astronomy, University of Michigan, 1085 S. University, Ann Arbor, MI 48109, USA <sup>7</sup> Institute of Physics, École Polytechnique Fédérale de Lausanne (EPFL), Observatoire de Sauverny, 1290 Versoix, Switzerland <sup>8</sup> Kavli Institute for Astrophysics and Space Research, Massachusetts Institute of Technology, 77 Massachusetts Ave., NE83-569, Cambridge, MA 02139, USA Space Telescope Science Institute, 3700 San Martin Dr., Baltimore, MD 21218, USA <sup>10</sup> Smithsonian Astrophysical Observatory, MS 4, 60 Garden St., Cambridge, MA 02138, USA Departamento de Astronomia, Universidad de Concepcion, Casilla160-C, Concepcion, Chile <sup>12</sup> Smithsonian Astrophysical Observatory, MS 67, 60 Garden St., Cambridge, MA 02138, USA CHARA Array of the Georgia State University, Mount Wilson, CA 91023, USA 14 Max-Planck-Institut für Astronomie, Königstuhl 17, 69117 Heidelberg, Germany <sup>15</sup> School of Physics and Astronomy, Astrophysics Group, University of Exeter, Stocker Road, Exeter, EX4 4QL, UK Received 2024 April 16; revised 2024 June 19; accepted 2024 June 20; published 2024 September 3

#### **Abstract**

The Cepheid AW Per is a component in a multiple system with a long-period orbit. The radial velocities of Griffin cover the 38 yr orbit well. An extensive program of interferometry with the Center for High Angular Resolution Astronomy array is reported here, from which the long-period orbit is determined. In addition, a Hubble Space Telescope high-resolution spectrum in the ultraviolet demonstrates that the companion is itself a binary with nearly equal-mass components. These data combined with a distance from Gaia provide a mass of the Cepheid (primary) of  $M_1 = 6.79 \pm 0.85 \, M_{\odot}$ . The combined mass of the secondary is  $M_{\rm S} = 8.79 \pm 0.50 \, M_{\odot}$ . The accuracy of the mass will be improved after the fourth Gaia data release, expected in approximately two years.

*Unified Astronomy Thesaurus concepts:* Cepheid variable stars (218); Multiple stars (1081); Stellar masses (1614); Stellar evolution (1599)

# 1. Introduction

The quest for masses of Cepheid variable stars starts with the identification of binary or multiple systems of which they are members. In the case of the Cepheid AW Per, the possibility of a companion has been suggested both by photometry and radial velocities (RVs). Oosterhoff (1960) suggested a hot companion could explain the relatively small photometric amplitude in the ultraviolet. Miller & Preston (1964) obtained spectra and identified a composite spectrum made up of the Cepheid and hot companion. The resultant spectrum had a combined Ca II H (Cepheid) plus H $\epsilon$  (companion) feature which is deeper than the Ca II K line from the Cepheid alone. Lloyd Evans (1968) was the first to find orbital motion in the system by comparing the velocities from Miller & Preston (1964) with earlier velocities from Joy (1937).

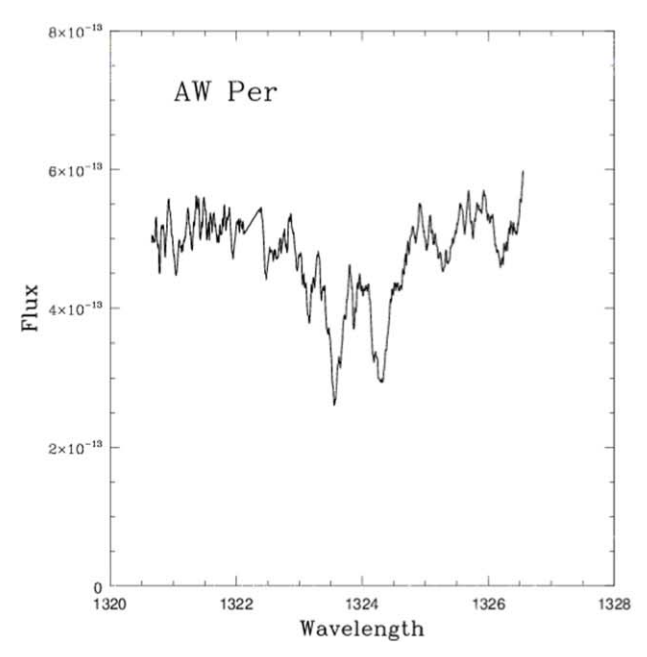
Not surprisingly, many people over many seasons provided velocities for an orbit, which ultimately proved to be about

Original content from this work may be used under the terms of the Creative Commons Attribution 4.0 licence. Any further distribution of this work must maintain attribution to the author(s) and the title of the work, journal citation and DOI.

40 yr (Welch & Evans 1989; Evans et al. 2000, and references therein). The difficulty of combining velocities from many instruments over a period this long was overcome by Griffin (2016) in a series of observations each year from 1976 to 2016 with the Cambridge RV spectrometer. This comprehensive data string has produced a definitive spectroscopic orbit. The Griffin paper also contains an extensive summary of all observations of AW Per (of which only a summary is provided here).

Many developments since the discovery of a companion have helped toward the ultimate goal of deriving a Cepheid mass. Oosterhoff (1960) and Miller & Preston (1964) correctly identified the companion as a late B star. Satellite ultraviolet spectroscopy provides a spectrum of the hot companion which is essentially uncontaminated by the Cepheid for wavelengths shorter than 1700 Å. An International Ultraviolet Explorer (IUE) low-resolution spectrum has been discussed several times (Böhm-Vitense & Proffitt 1985; Evans 1989; Welch & Evans 1989; and Massa & Evans 2008), partly because of revised software (Evans 1994). The temperature of the companion is revisited below based directly on the comparison with Kurucz ATLAS9 atmospheres. Both the temperature inferred for the companion and the orbit have changed somewhat throughout various analyses. However, the conclusion originally put forward by Welch & Evans (1989), that the mass function from the orbit and a reasonable mass estimate for the Cepheid require a companion mass larger than that of a

<sup>\*</sup> Based on observations with the NASA/ESA Hubble Space Telescope obtained at the Space Telescope Science Institute, which is operated by the Association of Universities for Research in Astronomy, Inc., under NASA contract NAS5-26555.



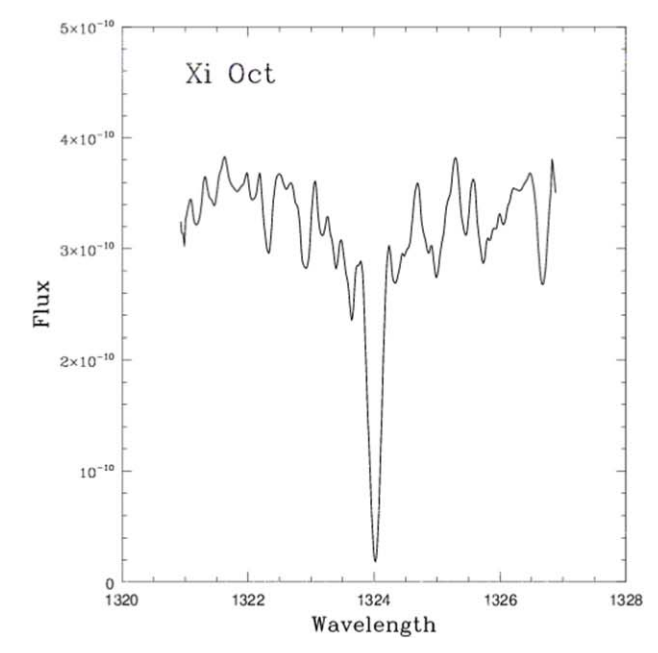


**Figure 1.** Left: the spectrum of the hot companion AW Per B in the region of the C II line 1324 Å. Right: the spectrum of the B6 IV star  $\xi$  Oct in the same region. The AW Per spectrum has a 10-point boxcar smoothing. Wavelength is in ångstroms; flux is in erg cm<sup>-2</sup> s<sup>-1</sup> Å<sup>-1</sup>.

single main-sequence companion, remains. Thus, the most direct interpretation is that the companion is itself a binary. This question is also discussed further below.

To derive a mass for the Cepheid, measured values of the inclination and the angular separation in arcseconds need to be added to the parameters of the Cepheid orbit. Two new approaches have added these. First, Massa & Evans (2008) observed the AW Per system with the Hubble Space Telescope (HST) Space Telescope Imaging Spectrograph (STIS), observing the system with three satellite roll angles. This allowed them to measure the separation and position angle. This observation is discussed in Section 3.2 (with a small update).

The second approach came from interferometry with the Center for High Angular Resolution Astronomy (CHARA) Array. Data analyzed using the CANDID software package resolved the system (Gallenne et al. 2015).

The Cepheid AW Per pulsates in the fundamental mode with a period of 6.4 days. In addition to the three stars making up the primary and the binary secondary, Kervella et al. (2019b) have identified an additional probable bound companion at an apparent separation of 8400 au, which has a spectral type of approximately K3.5 V.

This paper contains sections on the ultraviolet spectra (Section 2), both the HST high-resolution spectra and an IUE low-resolution spectrum, followed by CHARA interferometry (Section 3), fitting the orbit (Section 4), including the Cepheid mass, and discussion of the results (Section 5). Conclusions are given in the final section (Section 6).

### 2. Ultraviolet Spectra

### 2.1. High-resolution Spectra

In order to explore the companion further, high-resolution echelle ultraviolet STIS spectra were obtained with HST, where the hot companion AW Per B dominates completely. The observations have a central wavelength of 1416 Å and cover approximately 1325–1500 Å. They were obtained over six

orbits between JD 2457301.9927 and 2457303.1391 for a total exposure time of 15,810 s.

The echelle orders were combined using an appropriate blaze function, producing a one-dimensional spectrum. Interstellar lines (narrower than stellar lines) were removed by interpolation. Details of the reduction are discussed for the V350 Sgr system (Evans et al. 2018a), including coadding the spectra from the six orbits into a single spectrum.

These spectra were compared with that of  $\xi$  Oct = HD 215573 using a spectrum from the Astral Hot Stars project (Ayres 2010), a collection of carefully processed high-signal-to-noise (S/N), high-resolution STIS spectra. <sup>16</sup>  $\xi$  Oct is listed in this atlas as a B6 IV sharp-lined "normal" B star (V = 5.31 mag; B - V = -0.12 mag). It is a "slowly pulsating B star," a class which has nonradial g-mode pulsations (albeit with small magnitude variations). One reason  $\xi$  Oct was selected is that its parameters including temperature have been well determined by Fitzpatrick & Massa (2005).

The first inspection of the spectra of AW Per and  $\xi$  Oct presents a striking contrast (Figure 1). The C II line at 1324 Å has the profile of a deep line in  $\xi$  Oct. AW Per has two separated but fairly narrow lines; that is, both components of the binary companion Ba and Bb have been detected with a substantial velocity difference.

In Figure 1, the depths of the red and blue components of AW Per B are nearly equal, implying that the two stars Ba and Bb are similar in temperature and luminosity. As an exploration of the properties of the components of the binary companion, the spectrum of  $\xi$  Oct has been used. The temperature of  $\xi$  Oct has been determined to be  $14,347\pm138\,\mathrm{K}$  by Fitzpatrick & Massa (2005) from the energy distribution, including IUE spectra. This is comparable to the temperature of AW Per found in Section 2.2. An important part of the current study is to determine the properties of both stars in the binary companion as far as possible. In this exploration the

https://casa.colorado.edu/~ayres/ASTRAL/

Table 1
Companion Velocities

		Compa	nion velocities		
$\lambda$	λ	$V_B$	±	$V_R$	±
Start	End	1.	. 1.	. 1.	
(Å)	(Å)	$(km s^{-1})$	$(\text{km s}^{-1})$	$(\text{km s}^{-1})$	$(\text{km s}^{-1})$
1321	1331	-87.7	0.5	71.0	0.4
1334	1338	•••	•••	7.2	9.6
1338	1348	-110.2	19.1	79.6	28.9
1348	1355	-73.8	1.3	84.2	0.5
1355	1365	-53.2	1.8	66.4	1.9
1365	1371	-89.5	0.1	85.4	0.1
1371	1378	-93.4	5.7	86.8	3.5
1378	1386	-71.9	0.7	91.7	1.5
1386	1395	-29.1	1.8	84.8	0.7
1395	1402	-79.2	14.9	83.8	2.9
1402	1412	-109.0	54.7	70.1	11.0
1412	1418	-84.3	0.4	86.5	0.4
1418	1428	-76.6	0.1	70.2	0.1
1428	1437	-78.1	1.0	71.7	0.8
1437	1449	-79.5	3.0	86.9	3.0
1449	1458	-92.0	12.8	83.5	7.6
1458	1467	-88.2	2.4	78.2	1.4
1467	1472	-69.4	4.3	73.6	3.1
1472	1482	-73.9	2.4	81.5	0.9
1482	1490	-60.9	29.3	93.7	29.8
1490	1498	-66.4	0.6	78.4	0.5
1498	1506	-90.0	2.1	80.6	1.5
1506	1512	-69.6	14.1	76.8	13.5

temperatures of AW Per B and  $\xi$  Oct are similar enough for an initial examination.

Velocities on the coadded STIS spectrum were measured in the same way as for V350 Sgr using cross-correlation. In this case, a synthetic spectrum approximating a B7 star with a temperature of 13,000 K and a surface gravity log g of 4.0 was used, which responded to both components. It was generated from the synthetic spectrum code SYNTHE (Kurucz 2017) with an ATLAS9 stellar atmosphere model (Castelli & Kurucz 2003; Kurucz 2017).

Velocities of both components (B blue and R red for blueshifted and redshifted components, respectively) for each wavelength region are listed in Table 1 and shown in Figure 2. A mean velocity was computed for each component, omitting wavelength regions where either component had a standard deviation larger than  $10~\rm km~s^{-1}$  (as well as one region with a very discordant velocity). All standard deviations were set to at least  $0.5~\rm km~s^{-1}$ . The results are  $-80.6\pm2.2$  and  $79.0\pm1.8~\rm km~s^{-1}$ , with a velocity difference of  $158.6\pm2.8$ .

A spectrum approximating the two components of AW Per B was created from  $\xi$  Oct, adding two spectra separated by 159 km s<sup>-1</sup>, the velocity separation between the components. Because the blue component is slightly deeper than the red component, they are designated Ba and Bb, respectively. Four versions of the summed spectrum were created with a ratio between the components f(Ba)/f(Bb) of 0.95, 1.05, 1.10, and 1.15. The best agreement is for a ratio of 1.05, shown in Figure 3. Thus, the line depths, and hence presumably the fluxes at 1324 Å, differ by only a small amount.

# 2.2. Low-resolution Spectra

AW Per was observed with the IUE satellite in low-resolution mode (resolution 6 Å). The spectrum SWP 27541 is discussed here. The high-resolution STIS spectrum discussed

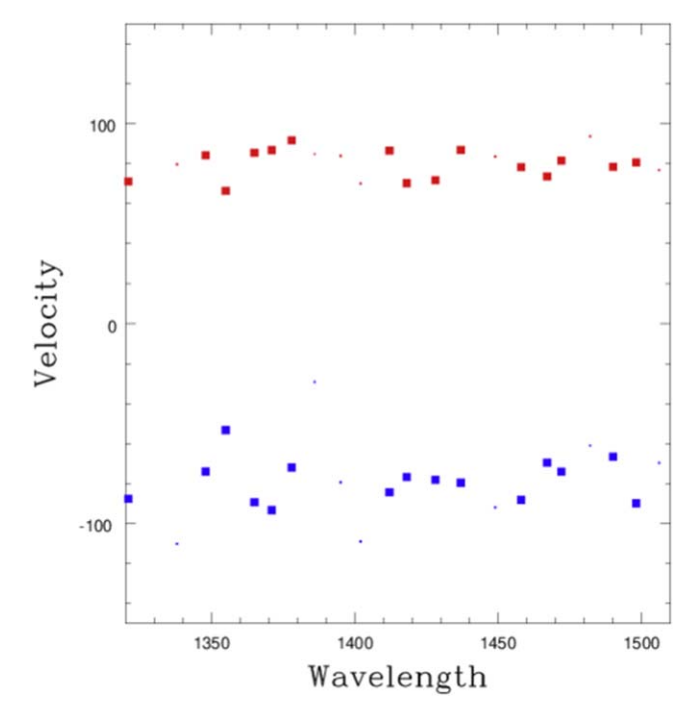


**Figure 2.** Velocities for the two components of the AW Per spectrum. Colors correspond to red and blue velocity components. Large squares are used in the means; dots are velocities which were rejected because of large errors (see text). Wavelength is in ångstroms; velocities are in kilometers per second.

in Section 2.1 permits the identification of the two components of the B component (Ba and Bb). In low resolution they are not resolved. Since Ba and Bb are very similar in temperature and luminosity, we determine a single temperature from the composite spectrum in this section.

$$2.2.1. E(B - V)$$

The first consideration in interpreting an ultraviolet spectrum is determining the reddening. In particular, for AW Per, early discussions of the IUE spectrum (Evans 1989) incorporated both a substantial E(B-V) (0.52 mag) and also a significant contribution from the companion. We revisit this topic briefly here. Moffett & Barnes (1985) provide an extensive catalog of Cepheid observations in the Johnson system, from which Groenewegen (1999) provided a transformed I magnitude in the Cousins system.

Anticipating the result below, as a first exploration we use a companion temperature of 14,000 K, based on E(B - V) = 0.52(Evans 1994). The absolute magnitude for the Cepheid is calculated from the period (6.4636 days) and the periodluminosity law (Leavitt law) in V from Cruz Reyes & Anderson (2023),  $M_V = -3.89$  mag. This is based on Gaia Data Release 3 (DR3) parallaxes of Cepheids and open clusters. The temperature of the companion corresponds closely to a B7 mainsequence star in the calibration of Pecaut & Mamajek (2013), providing colors of B - V = -0.128 mag and V - I = -0.133. This corresponds to an absolute magnitude  $M_V = -0.9 \,\mathrm{mag}$ (Drilling & Landolt 2000), making the companion 2.99 mag fainter than the Cepheid in V. The colors of the companion are then reddened to the E(B-V) of the Cepheid, becoming B - V = 0.392 mag and (V - I) = 0.517 mag, and from these the B and I of the companion are created (Table 2). From the  $\langle B \rangle - \langle V \rangle$  and  $\langle V \rangle - \langle I \rangle$  colors, the E(B - V) is calculated using

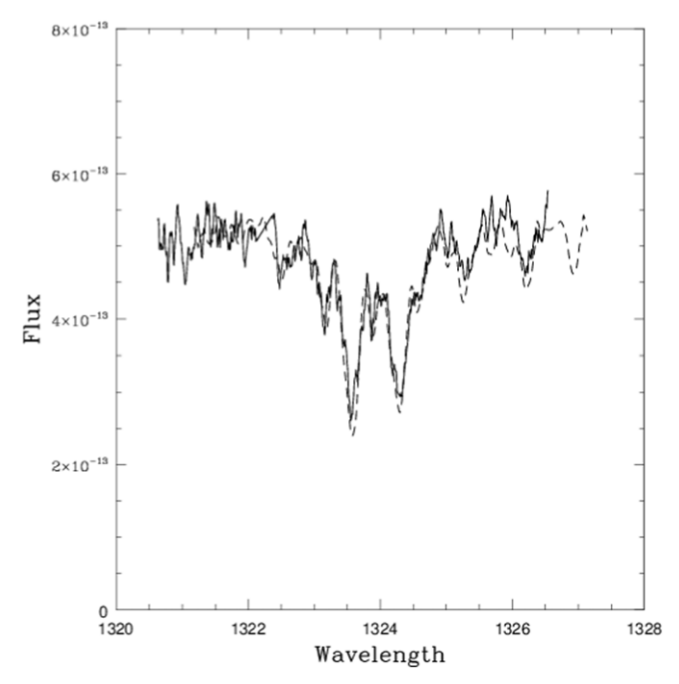


**Figure 3.** The AW Per spectrum (solid line) compared with a simulated spectrum created from the  $\xi$  Oct spectrum (dashed line). See text for details. The AW Per spectrum has a 10-point boxcar smoothing. Wavelength is in ångstroms; flux is in erg cm<sup>-2</sup> s<sup>-1</sup> Å<sup>-1</sup>.

Table 2
Correction for Companion

	$\langle B \rangle$	$\langle V \rangle$	$\langle I \rangle$
Comp: 1 B7 Star			
Comp	10.868	10.476	9.959
Cep + Comp	8.540	7.486	6.227
Сер	8.675	7.557	6.260
Comp: 2 B7 Stars			
Comp	10.118	9.726	10.243
Cep + Comp	8.540	7.486	6.227
Cep	8.829	7.634	6.256

the appropriate formula from Fernie (1990) for a  $BV(I)_C$  system to be 0.452 mag (Table 3).

From the discussion of the HST high-resolution spectra in Section 2.1, the companion is made up of two stars of nearly equal temperature and mass. The effect of two stars of equal temperature is shown in Table 2 below. The reddening values from the models of the companion based on one or two hot stars are quite similar (Table 3). For comparison, the E(B-V) before correcting for the effect of the companion is included. The last line in Table 3 is the reddening from Fernie (1990), which is a little different since it is the average from photometric systems. Groenewegen (2018) recommends scaling the Fernie reddenings by 0.94, which is close to 0.50.

## 2.2.2. Companion Temperature

The IUE spectrum has been reanalyzed here using Kurucz ATLAS9 BOSZ atmospheres (Bohlin et al. 2017) This was done in the same way as for detached eclipsing binaries (DEBs) containing hot stars (Evans et al. 2023).

The region between 1250 and 1350 Å has several strong lines from low-excitation states from Si II and C II, which are apparent in Figure 4. The Si II lines have been shown to be

Table 3
Reddening

	$\langle B \rangle - \langle V \rangle$	$\langle V \rangle  -  \langle I \rangle$	E(B-V)
Comp: 1 B7 star	1.118	1.297	0.452
Comp: 2 B7 stars	1.195	1.378	0.495
Uncorrected	1.054	1.259	0.457
Fernie	•••	•••	0.522

temperature sensitive (Massa 1989). In the low-resolution spectrum we have not attempted to model them, but regard them as an extra source of uncertainty in the fit. In AW Per, for example, the lines are made up of two components separated in velocity, making modeling beyond the scope of the low-resolution spectrum discussion.

The IUE spectrum was dereddened using  $E(B-V)=0.50\,\mathrm{mag}$  (Table 3). Comparisons with the models (spectral fits) are shown in Figure 4; the differences between the spectrum and the models are shown in Figure 5. The resulting temperature was  $14,036\pm1079\,\mathrm{K}$  from the parabola fit to the standard deviations of the spectrum-model differences (Figure 6). As in the discussion of the DEBs, the uncertainty was also estimated visually from the spectral differences (Figure 5) to be 500 K. This temperature is sufficiently close to the input temperature used in estimating the effect of the companion on the reddening that no further iteration is necessary. As discussed in Evans et al. (2023), the temperature is only mildly sensitive to E(B-V) because of the relatively small wavelength range of the spectrum and the structure in the energy distribution.

The study of the DEBs combined the temperatures with their masses to produce a mass-temperature relation. Since the two components of the B system Ba and Bb are essentially identical, the temperature here directly provides masses for both. This is discussed further in Section 5.

### 3. Relative Astrometry

### 3.1. CHARA Interferometry

#### 3.1.1. Data Acquisition

Long-baseline optical interferometric data were collected with the Michigan InfraRed Combiner (MIRC; data before 2017.5; Monnier et al. 2004) and the Michigan InfraRed Combiner-eXeter (MIRC-X; data after 2017.5; Anugu et al. 2020), installed at the CHARA Array (ten Brummelaar et al. 2005) at the Mount Wilson Observatory. MIRC-X is actually an upgrade of the MIRC instrument, with mostly an improved sensitivity and wavelength coverage. In addition, recent improvements at CHARA include the commissioning of a new six-telescope beam combiner, the Michigan Young STar Imager at CHARA (MYSTIC; Monnier et al. 2018; Setterholm et al. 2023), designed alongside the MIRC-X upgrade and capable of simultaneous observations. The CHARA Array consists of six 1 m aperture telescopes with a Y-shaped configuration (two telescopes on each branch), oriented to the east (E1, E2), west (W1, W2), and south (S1, S2), and so offering a good coverage of the (u, v) plane. The baselines range from 34 to 331 m, providing an angular resolution down to 0.5 mas at  $\lambda = 1.6 \,\mu\text{m}$ .

MIRC combined the light coming from all six telescopes in the *H* band ( $\sim$ 1.6  $\mu$ m), with three spectral resolutions (R = 42,

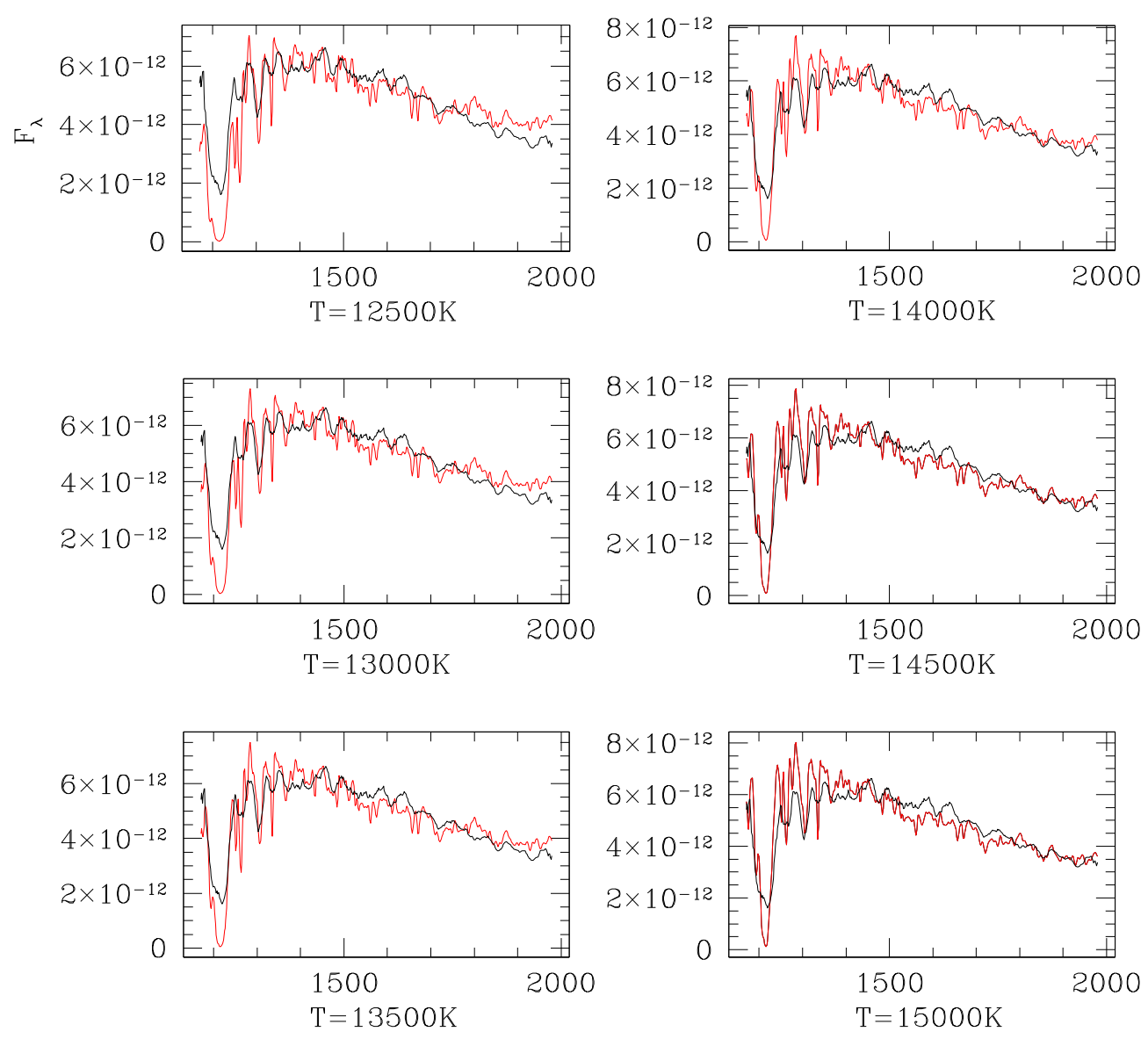


Figure 4. The comparison between the BOSZ models (red) and the IUE spectrum (black) dereddened with E(B-V)=0.50 mag. The wavelength (x-axis) is in ångstroms; the flux is in erg cm<sup>-2</sup> s<sup>-1</sup> Å<sup>-1</sup>. The temperature for the models is given beneath each panel. The region between 1180 and 1250 Å is shown in the plots, but is not included in the temperature determination because of contamination from interstellar Ly $\alpha$ . The region between 1250 and 1350 Å has several strong lines or multiplets of Si II and C II.

150, and 400). The recombination of six telescopes gives simultaneously 15 fringe visibilities and 20 closure-phase measurements, which are our primary observables. MIRC-X also combines the light from six telescopes, with spectral resolutions  $R=50,\,102,\,190,\,$  and 1170. Our MIRC and MIRC-X observations used only the lowest spectral resolution. MYSTIC is a K-band instrument working similarly to MIRC-X and offering spectral resolutions  $R=50,\,280,\,1000,\,$  and 1700. The log of our observations is available in Table 4.

We followed a standard observing procedure, i.e., we monitored the interferometric transfer function by observing a calibrator before and after our Cepheids. The calibrators were selected using the SearchCal software (Bonneau et al. 2011) provided by the Jean-Marie Mariotti Center. They are listed in Table 4.

17 http://www.jmmc.fr/searchcal

The data were reduced with the standard MIRC and MIRC-X pipelines (Monnier et al. 2007; Anugu et al. 2020). <sup>18</sup> (For 2019 and 2021–2022, the MIRC pipelines are versions 1.3.3 and 1.4.0, respectively.) The main procedure is to compute squared visibilities and triple products for each baseline and spectral channel, and to correct for photon and readout noises. The data acquired in 2012 October 1 are displayed in Figure 7. MYSTIC data are also reduced with the MIRC-X pipeline.

### 3.1.2. Data Analysis

To detect the companion, or to be more precise the center of light (in our specific case of a binary companion), we used the interferometric tool CANDID (Gallenne et al. 2015). <sup>19</sup> The

<sup>18</sup> https://gitlab.chara.gsu.edu/lebouquj/mircx\_pipeline

<sup>&</sup>lt;sup>19</sup> Available at https://github.com/amerand/CANDID and https://github.com/agallenne/GUIcandid for a GUI version.

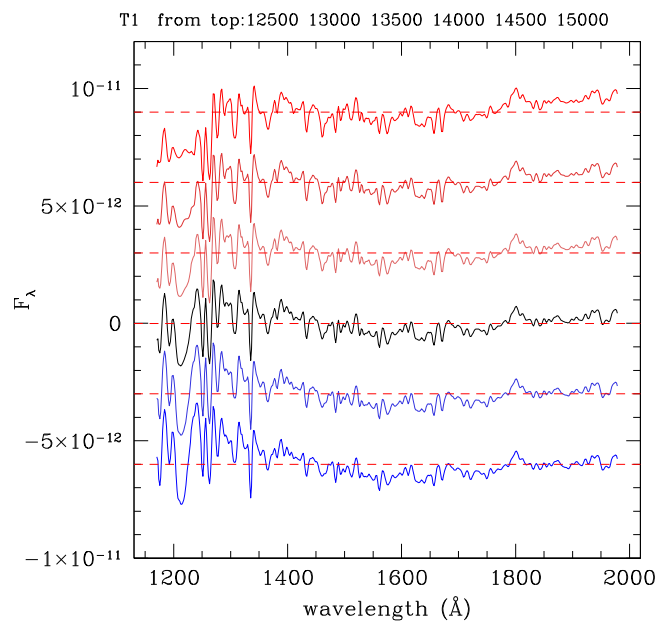


**Figure 5.** The difference between the model and the spectrum, dereddened by E(B-V)=0.50 mag. The temperatures for the models are listed at the top. The difference spectrum in black is the best fit.

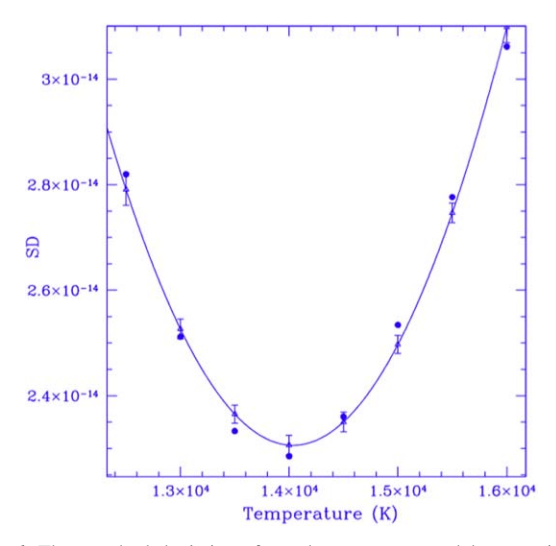


**Figure 6.** The standard deviations from the spectrum—model comparisons as the temperature of the models is changed. Dots are the standard deviation; triangles give the parabola fit.

main function allows a systematic search for companions performing an  $N \times N$  grid of fits, the minimum required grid resolution, which is estimated a posteriori in order to find the global minimum in  $\chi^2$ . The tool delivers the binary parameters, namely the flux ratio f and the relative astrometric separation  $(\Delta\alpha, \Delta\delta)$ , together with the uniform-disk angular diameter  $\theta_{\rm UD}$  of the primary star (the Cepheid). The angular diameter of the companion is assumed to be unresolved by the interferometer. The significance of the detection is also given, taking into account the reduced  $\chi^2$  and the number of degrees of freedom and comparing it with a single uniform-disk model that best fits the data. They are listed in Table 5, together with our measured astrometric positions. For the observations of 2015, we combined the data set in order to increase the detection

level. In this case, we only used the closure-phase measurements because of the variation of the angular diameter between these two observations ( $\sim \! 10\%$ , which was fixed to the average fitted value). For 2014 October, we also only used the closure phase because of a low detection level when including the squared visibilities, likely due to poor seeing conditions which mostly affect this observable.

Uncertainties on the fitted parameters are estimated using a bootstrapping function. From the distribution, we took the median value and the maximum value between the 16th and 84th percentiles as uncertainty for the flux ratio and angular diameter. For the fitted astrometric position, the error ellipse is derived from the bootstrap sample (using a principal component analysis). The angular diameters and astrometric positions were then multiplied by factors of  $1.004 \pm 0.0025$  mas for MIRC and divided by  $1.0054 \pm 0.0006$  mas for MIRC-X (J. D. Monnier 2024, private communication) to take into account the uncertainty from the wavelength calibration. This is equivalent to adjusting the respective wavelengths reported in the OIFITS files by the same factors. Uncertainty on the angular diameter measurements was estimated using the conservative formalism of Boffin et al. (2014) as follows:

$$\sigma_{\theta_{\rm UD}}^2 = N_{\rm sp} \sigma_{\rm stat}^2 + \delta \lambda^2 \theta_{\theta_{\rm UD}}^2,$$

where  $N_{\rm sp}$  is the number of spectral channels,  $\sigma_{\rm stat}^2$  the uncertainty from the bootstrapping, and  $\delta\lambda = 0.25\%$  or 0.06%, as mentioned above for MIRC and MIRC-X, respectively.

We measured a mean uniform-disk diameter in the H band of  $\theta_{\rm UD}=0.559\pm0.051$  mas (the standard deviation is taken as the uncertainty), which is in agreement at  $0.5\sigma$  with the value estimated by Trahin et al. (2021) from a spectrophotometric analysis. Using the Gaia DR3 parallax with the Lindegren et al. (2021) correction, this provides a linear radius of  $R=58.9\pm5.6\,R_\odot$ , also in agreement with Trahin et al. (2021). We also estimated an average flux ratio in H of  $f_{\rm H}=1.78\%\pm0.51\%$ . We have examined the variation of angular diameter as a function of pulsation phase. The range is approximately the  $\pm6\%$  expected for pulsation, but the phase range from 0.18 to 0.64 is too small for a definitive conclusion about whether it follows the pattern expected for pulsation.

We examined the astrometric residuals as a function of time. There is no sign of additional wobble which might be caused by the binary secondary.

# 3.2. Hubble Space Telescope/STIS

Massa & Evans (2008) observed the AW Per system with the HST/STIS spectrograph. By observing at three spacecraft roll angles, they were able to derive the separation and angle of components A and B. It has since been realized that the roll angle used in the analysis needs to be corrected, and the final result is now  $13.74 \pm 0.26$  mas at a position angle of  $274.16^{\circ} \pm 1.94^{\circ}$  (Figure 8).

# 4. Orbit

The AW Per system now has velocities providing good coverage of the 38 yr orbit. In addition, extensive interferometry now covers more than a quarter of the orbit, which provides both the separation between the Cepheid and the companion (itself a binary) and the inclination. The HST/STIS spectrophotometric spectra provided the surprise of a signal

 $<sup>^{\</sup>rm 20}$  The computer precision limits the conversion to S/N values greater than 8.

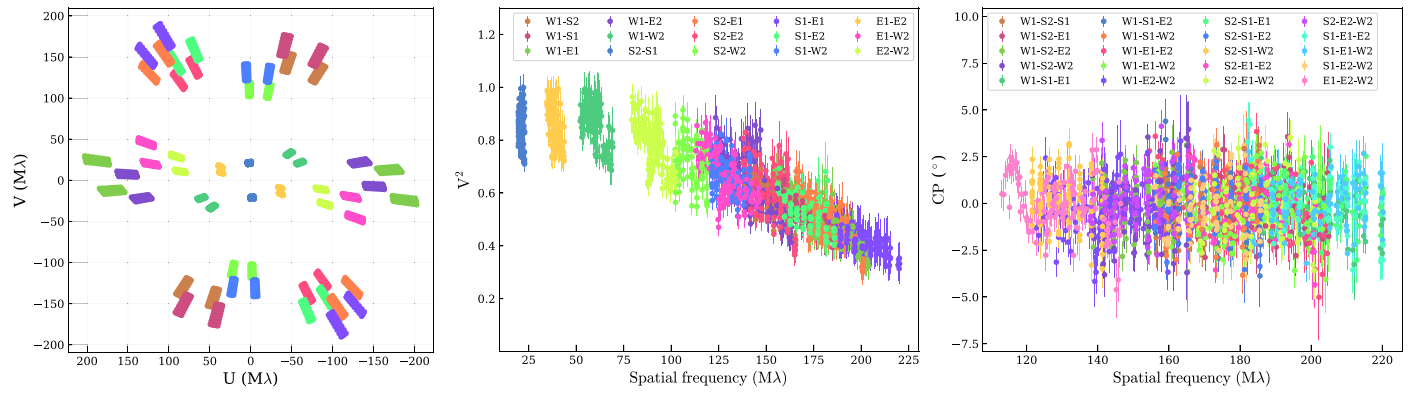


Figure 7. (u,v) coverage, squared visibilities, and closure-phase data for the observations of 2012 October 1.

 Table 4

 Log of Our MIRC, MIRC-X, and MYSTIC Observations

UT Date	JD	Inst.	$N_{ m spec}$	$N_{ m vis}$	$N_{\mathrm{CP}}$	Calibrators
2012 Oct 01	2456201.93097	MIRC	8	1657	2232	1, 2
2013 Sep 14	2456549.96703	MIRC	8	1735	2267	3, 4
2013 Sep 25	2456560.92238	MIRC	8	561	271	3, 4
2014 Oct 01	2456931.99035	MIRC	8	906	747	5, 6
2015 Oct 22	2457318.00959	MIRC	8	447	238	4, 5
2015 Oct 23	2457318.83962	MIRC	8	334	181	4, 5
2019 Oct 15	2458771.960780	MIRC-X	8	1080	1440	7, 8, 9
2021 Sep 20	2459477.955772	MIRC-X	8	2073	2555	7, 8, 9
2021 Sep 20	2459477.951951	MYSTIC	10	3378	4058	7, 8, 9
2022 Nov 19	2459902.807354	MIRC-X	8	3315	3021	10, 11

Notes.  $N_{\rm spec}$ : number of spectral channels.  $N_{\rm vis}$ : number of visibility measurements.  $N_{\rm CP}$ : number of closure-phase measurements. The calibrators used have the following angular diameters: 1:  $\theta_{\rm LD}({\rm HD~19845}) = 0.788 \pm 0.056$  mas; 2:  $\theta_{\rm LD}({\rm HD~30825}) = 0.564 \pm 0.040$  mas; 3:  $\theta_{\rm LD}({\rm HD~17573}) = 0.414 \pm 0.029$  mas; 4:  $\theta_{\rm LD}({\rm HD~25867}) = 0.551 \pm 0.039$  mas; 5:  $\theta_{\rm LD}({\rm HD~29645}) = 0.522 \pm 0.037$  mas; 6:  $\theta_{\rm LD}({\rm HD~30090}) = 0.521 \pm 0.037$  mas; 7:  $\theta_{\rm LD}({\rm HD~30099}) = 0.453 \pm 0.010$  mas; 8:  $\theta_{\rm LD}({\rm HD~280306}) = 0.427 \pm 0.009$  mas; 9:  $\theta_{\rm LD}({\rm BD~4~38.1014}) = 0.456 \pm 0.010$  mas; 10:  $\theta_{\rm LD}({\rm HD~30586}) = 0.464 \pm 0.010$  mas; 11:  $\theta_{\rm LD}({\rm HD~276662}) = 0.476 \pm 0.010$  mas.

 Table 5

 Relative Astrometric Position of the AW Per Companion

JD (day)	$\Delta \alpha$ (mas)	$\Delta\delta$ (mas)	$\sigma_{\mathrm{PA}}$ (deg)	$\sigma_{ m maj}$ (mas)	$\sigma_{\min} \pmod{\max}$	f (%)	$ heta_{ ext{UD}}$ (mas)	$n\sigma$
2456201.931	29.751	12.579	-176.2	0.076	0.033	$1.59 \pm 0.09$	$0.636 \pm 0.016$	>8
2456549.967	31.012	10.528	159.3	0.081	0.029	$1.31 \pm 0.06$	$0.512 \pm 0.036$	>8
2456560.922	31.189	10.466	-162.7	0.296	0.061	$1.79 \pm 0.37$	$0.520 \pm 0.067$	3.8
2456931.990	32.116	8.026	-156.3	0.112	0.042	$1.28 \pm 0.18$	0.634	7.4
2457318.359	32.696	5.362	146.2	0.190	0.091	$2.34 \pm 0.61$	0.583	7.5
2458771.961	31.386	-4.714	-176.2	0.021	0.006	$1.21 \pm 0.04$	$0.505 \pm 0.007$	>8
2459477.956	29.060	-9.509	157.9	0.048	0.032	$2.69 \pm 0.23$	$0.588 \pm 0.019$	>8
2459477.952	29.058	-9.487	54.0	0.037	0.025	$3.03 \pm 0.21^{a}$	$0.622 \pm 0.028$	>8
2459902.807	27.320	-12.223	-145.7	0.092	0.049	$2.05\pm0.37$	$0.531\pm0.025$	3.2

#### Note.

from both the hot stars in the companion binary. This combination plus a distance provides complete information about the Cepheid orbit.

### 4.1. Pulsation Period

Light curves of Cepheids, and in particular AW Per, have been discussed extensively by Csörnyei et al. (2022). The authors detected the light time in the long-period orbit. The light-time effect is  $\pm 0.05$  day. Over the 15,000 days of the

Griffin observations, this corresponds to  $\leq$ 0.01 in phase, which will not affect the orbital solution.

Csörnyei el al. (2022) also show a parabola in the O-C diagram, presumably an evolutionary change. The period change is smaller than the light-time effect,  $0.113 \pm 0.024 \, \mathrm{s} \, \mathrm{yr}^{-1}$ . We have checked to see what the difference in phase is for the span of the Griffin observations for the evolutionary period change. This uses the coefficients of the parabola in the O-C diagram (G. Csörnyei 2023, private communication). The difference in phase between a constant period and a changing period is

<sup>&</sup>lt;sup>a</sup> The flux ratio for this observation was measured in the K band using MYSTIC. All other flux ratios are in the H band.

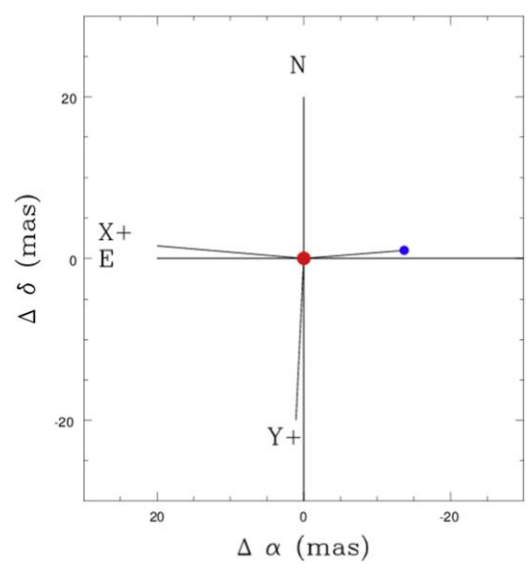


**Figure 8.** The orientation of the AW Per AB system. The figure shows the orientation of the STIS field for the roll angle in Massa & Evans (2008) of 175.526°, where the *x*-axis is the direction of the dispersion. The red dot is the Cepheid AW Per A and the blue dot is the companion AW Per B (itself a binary).

0.0116. This corresponds to  $\leq$ 0.5 km s<sup>-1</sup> in pulsation velocity, often significantly less, which adds very little to the uncertainties in the Griffin data. For this reason, we use a constant period in fitting the pulsation velocity curve.

The period found in the model fitting solution below  $6.463635 \pm 0.000006$  days (using the epoch from Griffin) corresponds to  $\leq 0.01$  difference in phase from the period of Csörnyei et al. (2022) over the span of the Griffin observations.

## 4.2. Model Fitting

Orbital parameters are determined by simultaneously fitting the RVs of the primary star (the Cepheid, which is a single-line spectroscopic binary) and the astrometric positions using a Markov Chain Monte Carlo (MCMC, 100 000 samples with uniform priors) routine. <sup>21</sup> Our RV model includes the pulsation of the Cepheid and its orbital reflex motion due to the presence of a companion, while the astrometric model defines the relative astrometric motion of the companion around the Cepheid. Our fitting procedure is detailed in Gallenne et al. (2018), who used a linear parameterization technique to solve for the orbital and pulsation parameters. Briefly, the RVs are defined by the combination of the pulsation and orbital motion with

$$V(t) = C_1 \cos \nu + C_2 \sin \nu + v_0 + \sum_{i=1}^{6} [A_i \cos(2\pi i \phi_{\text{puls}}) + B_i \sin(2\pi i \phi_{\text{puls}})],$$
 (1)

with  $\nu$  the true anomaly of the companion, the pulsation phase  $\phi_{\rm puls} = (t-T_0)/P_{\rm puls}$  (modulo 1) related to the pulsation period and the time of periastron passage, and  $(A_i, B_i)$  the amplitude of the Fourier series. The parameters  $C_1$ ,  $C_2$ , and  $v_0$  are related to the Keplerian elements through the relations of Wright &

Howard (2009):

$$K_{l} = \sqrt{C_{l}^{2} + C_{2}^{2}},$$

$$\tan \omega = \frac{-C_{2}}{C_{l}},$$

$$v_{\gamma} = v_{0} - K_{l}e \cos \omega$$

with  $K_1$  the semi-amplitude of the Cepheid's orbit due to the companion,  $\omega$  the argument of periastron of the companion's orbit, e the eccentricity of the orbit, and  $v_{\gamma}$  the systemic velocity.

The astrometric positions of the companion as measured from interferometry are modeled with the following equations:

$$\Delta \alpha = r[\cos \Omega \cos(\omega + \nu) - \sin \Omega \sin(\omega + \nu) \cos i], \quad (2)$$

$$\Delta \delta = r[\sin \Omega \cos(\omega + \nu) + \cos \Omega \sin(\omega + \nu) \cos i], \quad (3)$$

with a the angular semimajor axis in arcseconds,  $\Omega$  the position angle of the ascending node, and i the orbital inclination. The true anomaly  $\nu$  and the separation r at a given time t are calculated as

$$r = a(1 - e \cos E),$$
  
$$\tan \frac{\nu}{2} = \sqrt{\frac{1+e}{1-e}} \tan \frac{E}{2},$$

where the eccentric anomaly E is calculated by solving the Kepler's equation  $2\pi(t - T_p)/P_{\text{orb}} = E - e \sin E$ .

We used the RVs from Griffin (2016), which span the full orbital period of 40 yr. We did not add additional data from the literature to avoid possible systematics due to zero-point offsets.

AW Per is a single-line spectroscopic binary, therefore the masses and the distance are degenerate parameters. However, we can assume the distance and derive the individual masses (or in our case the primary mass and the total mass of the binary companion). We took the parallax measured by Gaia DR3 including the Lindegren correction,  $\varpi=1.0206\pm0.0287$  mas, which we implemented in our MCMC analysis with a normal distribution centered on 1.0206 mas with a standard deviation of 0.0287 mas. Masses are then derived from the distribution with

$$\begin{split} M_{\rm T} &= \frac{a^3}{P_{\rm orb}^2 \ \varpi^3}, \\ q &= \left[ \frac{a \sin i}{0.03357 \ \varpi \ K_1 \ P_{\rm orb} \sqrt{1 - e^2}} - 1 \right]^{-1}, \\ K_2 &= \frac{K_1}{q}, \\ M_1 &= \frac{M_{\rm T}}{1 \ + \ q}, \\ M_2 &= q \ M_1, \end{split}$$

with  $M_{\rm T} = M_1 + M_2$  the total mass in solar masses, a and  $\varpi$  in milliarcseconds,  $P_{\rm orb}$  in years,  $K_1$  in kilometers per second, and  $q = M_2/M_1$  the mass ratio. Our orbital fit is displayed in Figure 9 and the final parameters are listed in Table 6. Our fitted spectroscopic orbital elements are in very good agreement with those found by Griffin.

 $<sup>\</sup>overline{^{21}}$  With the Python package emcee developed by Foreman-Mackey et al. (2013).

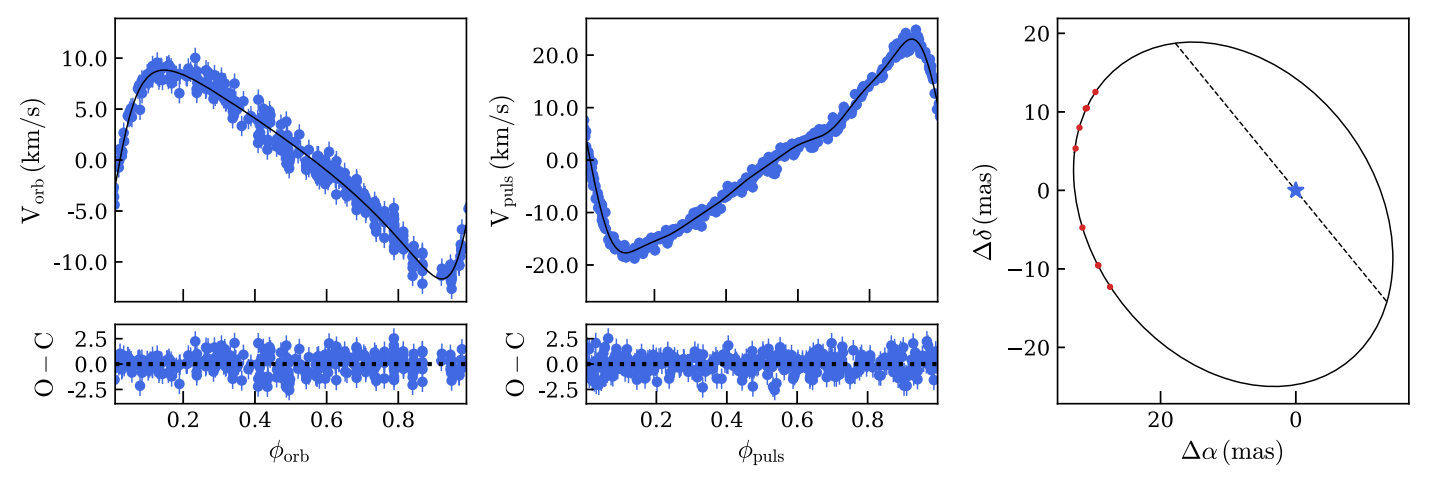


Figure 9. Result of our combined fit. Left: fitted (solid lines) and measured (blue dots) Cepheid's orbital velocity. Middle: fitted and measured pulsation velocity. Right: relative astrometric orbit of AW Per AB. Red points from CHARA.

 Table 6

 Final Estimated Parameters of the AW Per System

	Pulsation		Orbit
$\overline{P_{\text{puls}}}$ (days)	$6.463635 \pm 0.000008$	P <sub>orb</sub> (days)	$13849.44 \pm 0.83$
$T_0$ (JD)	2451873.616 <sup>a</sup>	$T_{\rm p}$ (JD)	$2438763.53 \pm 1.21$
$A_1  (\text{km s}^{-1})$	$3.62 \pm 0.02$	e	$0.465 \pm 0.002$
$B_1  (\text{km s}^{-1})$	$-14.93 \pm 0.01$	$\omega$ (deg)	$251.73 \pm 0.05$
$A_2  (\text{km s}^{-1})$	$2.23 \pm 0.01$	$K_1  ({\rm km  s}^{-1})$	$10.260 \pm 0.023$
$B_2  ({\rm km \ s}^{-1})$	$-7.09 \pm 0.01$	$v_{\gamma}  (\mathrm{km \ s}^{-1})$	$7.937 \pm 0.013$
$A_3  (\text{km s}^{-1})$	$0.51 \pm 0.01$	$\Omega$ (deg)	$44.58 \pm 0.08$
$B_3  ({\rm km  s^{-1}})$	$-3.80 \pm 0.01$	i (deg)	$46.64 \pm 0.12$
$A_4  (\text{km s}^{-1})$	$0.49 \pm 0.01$	a (mas)	$28.781 \pm 0.043$
$B_4  ({\rm km \ s^{-1}})$	$-1.75\pm0.01$	<i>a</i> (au)	$28.188 \pm 0.802$
$A_5 (\mathrm{km s}^{-1})$	$0.40 \pm 0.01$	$\varpi$ (mas)	$1.021 \pm 0.029^{b}$
$B_5  (\text{km s}^{-1})$	$-1.02 \pm 0.01$	q	$1.29 \pm 0.09$
$A_6  (\text{km s}^{-1})$	$0.03 \pm 0.01$	$M_1 (M_{\odot})$	$6.79 \pm 0.85$
$B_6  (\text{km s}^{-1})$	$-0.51 \pm 0.01$	$M_2(M_{\odot})$	$8.79 \pm 0.50$

Notes. Index 1 designates the Cepheid and index 2 its companion.

## 5. Discussion

Several sources of uncertainty contribute to the error in the derived masses, which are discussed here.

The distance used in Table 6 is derived from Gaia DR3. This needs to be revisited when the final Gaia processing is available. However, for such a long orbital period the results are not as uncertain as for shorter periods. In addition, Khan et al. (2023) have discussed parallax uncertainties for comparatively bright stars ( $G \simeq 7 \text{ mag}$ ), which could add 3% to Gaia parallaxes. To give a sense of the uncertainty in masses due to the uncertainty in distance at the present time, a comparison is provided by the Leavitt law (period-luminosity relation) from Cruz Reyes & Anderson (2023), which is based on Cepheids in clusters as well as parallaxes, all from Gaia DR3. (The Leavitt law is used in *V* so that observed magnitudes can be corrected for the companion.) The  $M_V$  for AW Per from this is -3.893 mag, corresponding to a distance of 989 pc. A simple substitution of this distance in Kepler's third law yields a sum of the masses of 15.53  $M_{\odot}$  instead of 15.58  $M_{\odot}$  from the solution in Table 6.

The revised astrometry from HST (Figure 8) is now in general agreement with the CHARA astrometry (Figure 9). However, the uncertainty on the HST astrometry is larger than that of the CHARA astrometry. Since that point degrades the solution, it was omitted in the solution in Table 6. Inclusion of the HST astronomy results in a Cepheid mass of  $5.75 \pm 0.77 \, M_{\odot}$ .

The combination of the spectroscopic and astrometric orbits allows the determination of the mass of the Cepheid primary  $(6.79 \pm 0.85 \ M_{\odot})$  and the combined mass of the stars in the binary secondary  $(8.79 \pm 0.50 \ M_{\odot})$ .

The coming Gaia Data Release 4 (DR4; expected within 2 yr) will include an improved parallax value and absolute epoch astrometry of the displacement of the photocenter of the AW Per AB system over a period of  $\approx$ 6 yr. In combination with the interferometric orbit, the Gaia astrometry will provide important new constraints on the orbital parameters and total mass of the system.

From Section 2.2.2, the temperature of the companion AW Per B (the composite Ba+Bb) is  $14,036\pm500\,\mathrm{K}$ . Previous temperature determinations using the same IUE spectrum range from 15,739 K (Massa & Evans 2008) and 11,481 K (Evans 1994) from comparisons with IUE spectra of spectral standards, giving

<sup>&</sup>lt;sup>a</sup> Kept fixed to the value given in Griffin (2016).

<sup>&</sup>lt;sup>b</sup> Taken from Gaia DR3  $1.0566 \pm 0.0287$  mas plus Lindegren correction -0.036038 mas.

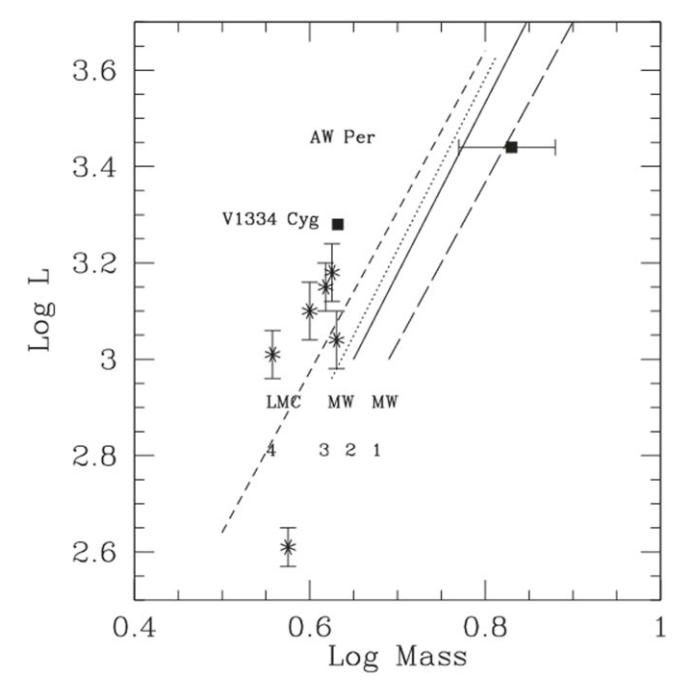


**Figure 10.** The mass–luminosity relation for Cepheids. Milky Way Cepheids (AW Per and V1334 Cyg), LMC Cepheids; asterisks. Predictions from evolutionary tracks: long dashed line: (1) MW metallicity, no main-sequence convective overshoot; solid line: (2) MW metallicity, moderate convective overshoot; dotted line: (3) MW metallicity, small convective overshoot and rotation; short dashed line: (4) LMC metallicity, moderate convective overshoot. Masses and luminosities are in solar units.

rise to a range of masses. The temperature found here is solidly in the middle.

The mass-temperature relation derived from DEBs (Evans et al. 2023) can be used to estimate the masses of the components of the B system, which are treated as essentially identical. Since Cepheid companions must be relatively young, they will be closer to the zero-age main sequence than the average DEB, and the mass-temperature relation is appropriately adjusted to be 0.02 smaller in  $\log M$  than that for DEBs. The mass of each component Ba and Bb is thus  $3.5\,M_\odot$ , ranging from 3.3 to  $3.7\,M_\odot$  for an uncertainty in T of 500 K.

The STIS echelle spectrum clearly shows the presence of both components (Figure 2), which provides unusually complete information for a triple system. The relative line strengths in Figure 1 provide an estimate of approximately 5% difference in flux. It is thus appropriate to estimate the mass of each component of AW Per B to be half that of  $M_2$  in Table 6 (4.4  $\pm$  0.5  $M_{\odot}$ ). The mass inferred from the temperature is close to this range.

A little more can be inferred about the properties of the AW Per B (Ba + Bb) binary system. The date of the STIS observations (JD 2457302) corresponds to a phase of 0.340 in the long-period orbit (Table 6). Using the mass ratio between the Cepheid and the AW Per B binary (q=1.3), the velocity of the center of mass of the AW Per B system is  $-3.8 \, \mathrm{km \, s^{-1}}$ , which is essentially zero in Figure 2. Thus, the velocity difference between components in Figure 2,  $\pm 79 \, \mathrm{km \, s^{-1}}$ , is approximately the orbital velocity. This velocity is consistent with a period approaching a year for the two masses in the short-period orbit. Such an orbit would have a semimajor axis approaching 2 au. This is, of course, a lower limit to the orbital velocity since it is from one random phase. In addition, the inclination is unknown. A larger orbital velocity would be

consistent with a shorter period and a smaller semimajor axis. Because the orbit with the Cepheid is so long, it can easily accommodate this orbit for the AW Per B.

Figure 10 shows the mass of AW Per in comparison with other masses for Cepheids from the Milky Way and the LMC. The luminosity for AW Per comes from the Gaia distance as used in Table 6 and the Cepheid magnitude and reddening from Tables 2 and 3. Uncertainty in the luminosity will be evaluated further after the Gaia DR4 release. In addition to AW Per, the other Milky Way Cepheid is V1334 Cyg (Gallenne et al. 2018), the most accurately determined Cepheid mass in the Milky Way. LMC Cepheids are from Pilecki et al. (2021). The predictions from evolutionary tracks cover a range of parameters: (1) MW metallicity, no main-sequence convective overshoot (Bono et al. 2016); (2) MW metallicity and moderate core convective overshoot (Bono et al. 2016); (3) MW metallicity, small convective overshoot and rotation (Anderson et al. 2016); and (4) LMC metallicity and moderate core convective overshoot (Bono et al. 2016). The error bars on the mass of AW Per are too large for it to be a definitive diagnostic between these parameters. This approach is preliminary until the final Gaia data release provides a definitive distance.

#### 6. Conclusions

In summary, the astrometry and velocity coverage of the long-period orbit provide a mass of the Cepheid AW Per. The accuracy of the mass of the Cepheid will improve with a distance from the final processing of Gaia data. The stars in the binary secondary AW Per Ba and Bb are well separated in velocity in the HST/STIS spectrum, which shows that they are very similar in mass.

# Acknowledgments

It is a pleasure to thank G. Csörynei for providing evolutionary period change from the O-C light-curve data and K. Frey for providing digital OCR versions of the Griffin velocities. D. Massa provided instructive conversations about the HST/STIS astrometry. Support for E.M.W. was provided from HST-GO-14194.001-A; support for C.P. and J.K. was provided from HST-GO-15861.001-A. H.M.G. was supported through grant No. HST-GO-15861.005-A from the STScI under NASA contract NAS5-26555. Support was provided to N.R.E. by the Chandra X-ray Center NASA Contract NAS8-03060

This work is based upon observations obtained with the Georgia State University Center for High Angular Resolution Astronomy (CHARA) Array at Mount Wilson Observatory. The CHARA Array is supported by the National Science Foundation under grant No. AST-1636624 and AST-2034336. Institutional support has been provided from the GSU College of Arts and Sciences and the GSU Office of the Vice President for Research and Economic Development. Time at the CHARA Array was granted through the NOIRLab community access program (NOIRLab PropID: 2019A-0071; PI: A. Gallenne). S.K. acknowledges funding for MIRC-X received from the European Research Council (ERC) under the European Union's Horizon 2020 research and innovation program (Starting grant No. 639889 and Consolidated grant No. 101003096). J.D.M. acknowledges funding for the development of MIRC-X (grant Nos. NASA-XRP NNX16AD43G,

NSF-AST 1909165) and MYSTIC (grant Nos. NSF-ATI 1506540, NSF-AST 1909165).

P.K., G.P., and W.G. acknowledge funding from the European Research Council (ERC) under the European Union's Horizon 2020 research and innovation program (projects CepBin, grant agreement No. 695099, and UniverScale, grant agreement No. 951549). A.G. acknowledges financial support from ANID-ALMA fund No. ASTRO20-0059. and the Agencia Nacional de Investigación Científica y Desarrollo (ANID) through the FONDECYT Regular grant No. 1241073. R.I.A. acknowledges support from the European Research Council (ERC) under the European Union's Horizon 2020 research and innovation program (grant Agreement No. 947660). R.I.A. is funded by the Swiss National Science Foundation through an Eccellenza Professorial Fellowship (award PCEFP2\_194638). R.M.R. acknowledges funding from the Heising-Simons Foundation 51 Pegasi b Fellowship.

This work has made use of data from the European Space Agency (ESA) mission Gaia (https://www.cosmos.esa.int/gaia), processed by the Gaia Data Processing and Analysis Consortium (DPAC; https://www.cosmos.esa.int/web/gaia/dpac/consortium). Funding for the DPAC has been provided by national institutions, in particular the institutions participating in the Gaia Multilateral Agreement. The SIMBAD database and NASA's Astrophysics Data System Bibliographic Services were used in the preparation of this paper.

The data presented in this article were obtained from the Mikulski Archive for Space Telescopes (MAST) at the Space Telescope Science Institute. The specific observations analyzed can be accessed via doi:10.17909/9gjn-gx79.

### **ORCID iDs**

Nancy Remage Evans https://orcid.org/0000-0002-4374-075X

Alexandre Gallenne https://orcid.org/0000-0001-7853-4094

Pierre Kervella https://orcid.org/0000-0003-0626-1749

John Monnier https://orcid.org/0000-0002-3380-3307

Richard I Anderson https://orcid.org/0000-0001-8089-4419

Charles Proffitt https://orcid.org/0000-0001-7617-5665

Wolfgang Gieren https://orcid.org/0000-0003-1405-9954

Joanna Kuraszkiewicz https://orcid.org/0000-0001-5513-029X

Narsireddy Anugu https://orcid.org/0000-0002-2208-6541

Rachael M. Roettenbacher https://orcid.org/0000-0002-

9288-3482 Benjamin R. Setterholm https://orcid.org/0000-0001-

5980-0246 benjamin R. Setterholm bittps://orcid.org/0000-0001-

Stefan Kraus https://orcid.org/0000-0001-6017-8773

#### References

```
Anderson, R. I., Saio, H., Ekström, S., Georgy, C., & Meynet, G. 2016, A&A,
   591, A8
Anugu, N., Le Bouquin, J.-B., Monnier, J. D., et al. 2020, AJ, 160, 158
Ayres, T. R. 2010, ApJS, 187, 149
Boffin, H. M. J., Hillen, M., Berger, J. P., et al. 2014, A&A, 564, A1
Bohlin, R. C., Meszaros, S., Fleming, S. W., et al. 2017, AJ, 153, 23
Böhm-Vitense, E., & Proffitt, C. 1985, ApJ, 296, 175
Bonneau, D., Delfosse, X., Mourard, D., et al. 2011, A&A, 535, A53
Bono, G., Braga, V. F., Pietrinferni, A., et al. 2016, MmSAI, 87, 358
Castelli, F., & Kurucz, R. L. 2003, in IAU Symp. 210, Modelling of Stellar
   Atmospheres, ed. N. Piskunov, W. W. Weiss, & D. F. Gray (San Francisco,
   CA: ASP), A20
Cruz Reyes, M., & Anderson, R. I. 2023, A&A, 672, A85
Csörnyei, G., Szabados, L., Molnár, L., et al. 2022, MNRAS, 511, 2125
Drilling, J. S., & Landolt, A. U. 2000, in Astrophysical Quantities, ed.
   A. N. Cox (London: Springer), 388
Evans, N. R. 1994, ApJ, 436, 273
Evans, N. R. 1989, AJ, 97, 1737
Evans, N. R., Ferrari, M. G., Kuraszkiewicz, J., et al. 2023, AJ, 166, 109
Evans, N. R., Proffitt, C., Carpenter, K. G., et al. 2018, ApJ, 866, 30
Evans, N. R., Vinko, J., & Wahlgren, G. M. 2000, AJ, 120, 407
Fernie, J. D. 1990, ApJS, 72, 153
Fitzpatrick, E. L., & Massa, D. 2005, AJ, 129, 164
Foreman-Mackey, D., Hogg, D. W., Lang, D., & Goodman, J. 2013, PASP,
Gallenne, A., Kervella, P., Evans, N. R., et al. 2018, ApJ, 867, 121
Gallenne, A., Mérand, A., Kervella, P., et al. 2015, A&A, 579, A68
Griffin, R. F. 2016, Obs, 136, 209
Groenewegen, M. A. T. 1999, A&AS, 139, 245
Groenewegen, M. A. T. 2018, A&A, 619, A8
Joy, A. H. 1937, AJ, 86, 363
Khan, S., Anderson, R. I., Miglio, A., Mosser, B., & Elsworth, Y. P. 2023,
     &A, 680, A105
Kervella, P., Gallenne, A., Evans, N. R., et al. 2019, A&A, 623, A117
Kurucz, R. L. 2017, ATLAS9: Model atmosphere program with opacity
   distribution functions, Astrophysics Source Code Library, ascl:1710.017
Lindegren, L., Bastian, U., Biermann, M., et al. 2021, A&A, 649, A4
Lloyd Evans, T. 1968, MNRAS, 141, 109
Massa, D. 1989, A&A, 224, 131
Massa, D., & Evans, N. R. 2008, MNRAS, 383, 139
Miller, J., & Preston, G. 1964, ApJ, 139, 1126
Moffett, T. J., & Barnes, T. G. 1985, ApJS, 58, 834
Monnier, J. D., Berger, J.-P., Millan-Gabet, R., & ten Brummelaar, T. A. 2004,
   Proc. SPIE, 5491, 1370
Monnier, J. D., Le Bouquin, J.-B., Anugu, N., et al. 2018, Proc. SPIE, 10701,
Monnier, J. D., Zhao, M., Pedretti, E., et al. 2007, Sci, 317, 342
Oosterhoff, P. T. 1960, BAN, 15, 199
Pecaut, M. J., & Mamajek, E. E. 2013, ApJS, 208, 9
Pilecki, B., Pietrzyński, G., Anderson, R. I., et al. 2021, ApJ, 910, 118
Setterholm, B. R., Monnier, J. D., Le Bouquin, J. B., et al. 2023, JATIS, 9,
ten Brummelaar, T. A., McAlister, H. A., Ridgway, S. T., et al. 2005, ApJ,
   628, 453
Trahin, B., Breuval, L., Kervella, P., et al. 2021, A&A, 656, A102
Welch, D. L., & Evans, N. R. 1989, AJ, 97, 1153
Wright, J. T., & Howard, A. W. 2009, ApJS, 182, 205
```